Supplementary Information

Nanometer-scale confinement of whispering gallery plasmonic modes excited by a plane wave

Henrik Parsamyan*, Roza Gabrielyan, Gurgen Arabajyan, Hovhannes Haroyan, and Khachatur Nerkararyan

Institute of Physics, Yerevan State University, A. Manoogian 1, Yerevan, 0025, Armenia

*Corresponding author: *hparsamyan@ysu.am*

I. MULTIPOLE DECOMPOSITION

To fully reveal the origin behind the strong enhancement of the electromagnetic energy, we apply multipole decomposition of the scattering spectra of split and solid GSP resonators based on spherical harmonics. The results are plotted in Fig. S1 (a) and (b), respectively, linked to the left axis. The right axis depicts the normalized total electromagnetic energy stored in the spacer.

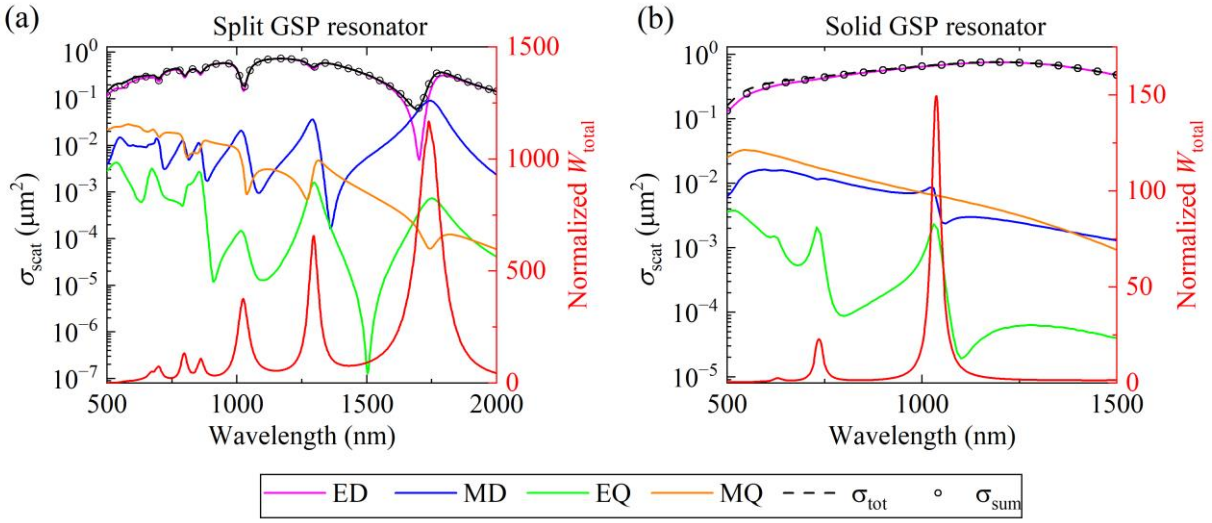

Fig. S1. Contributions of multipole components to the total scattering cross-section of (a) split and (b) solid GSP disk resonator linked to the left axis. The right axis in both plots shows the normalized total electromagnetic energy in the spacer. The disk diameter is 450 nm, spacer thickness is 10 nm, and the split width is 30 nm.

The multipole components are denoted as follows: ED-electric dipole (purple), MD-magnetic dipole (blue), EQ-electric quadrupole (green) and MQ-magnetic quadrupole (orange). σ_{sum} (black curve) represents the total sum of the multipole components: σ_{sum} = ED + MD + EQ + MQ. σ_{sim} is the numerically calculated total scattering cross-section.

A full set of expressions of the multipole components can be found elsewhere[1,2].

II. HYBRID MODES OF THE SPLIT GSP RESONATOR

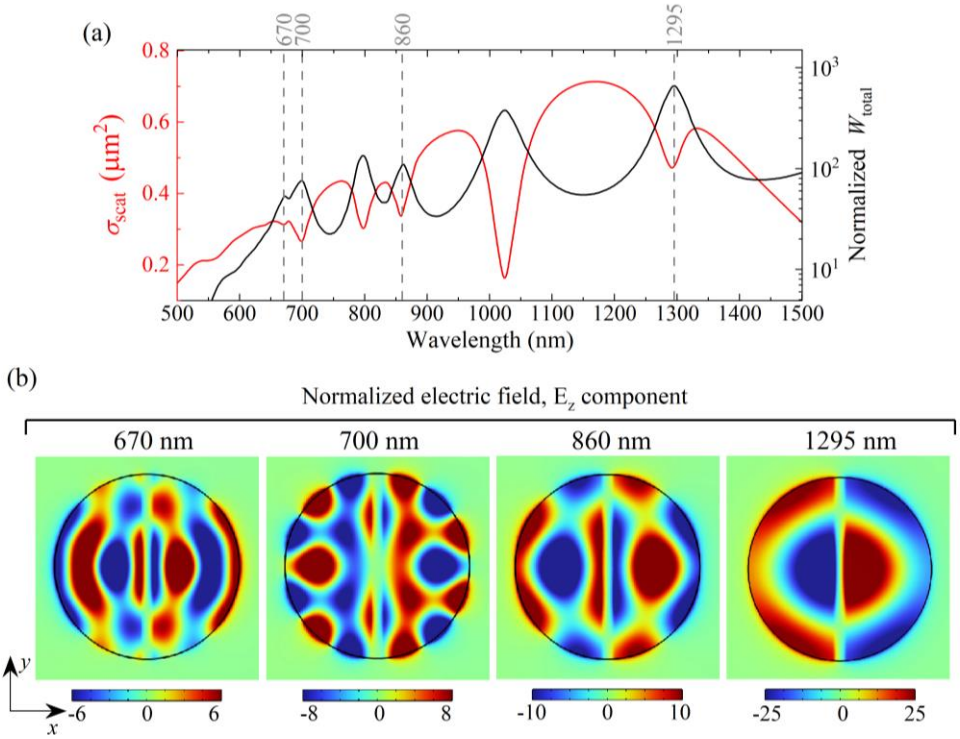

Fig. S2. (a) Spectra of the scattering (left) and normalized total energy (right) in the spacer of the split GSP resonator with diameter of 450 nm. Vertical dashed lines indicate the spectral positions of hybrid modes. (b) Distributions of the normalized amplitudes of the electric field E_z components of hybrid modes.

III. MODE PROFILE IN THE SOLID GSP RESONATOR

The profile of the normalized electric field Ez component of the (3,1) mode at 735 nm in the central XY plane of solid GSP configuration is depicted in Fig. S3. Here the field extrema are located deep within the dielectric spacer, in contrast to the split one. Due to high radial mode number ($\ell = 3$), a part of the field which extends into the surrounding air is relatively weak. Specifically, the $E_z/E_{z,max}$ ratio at the spacer-air interface is nearly 0.43, where $E_{z,max}$ is the maximum of the mode electric field. The exponential tail of this mode in the surrounding air drops by half at nearly 3.64 nm away from the resonator surface in the radial direction.

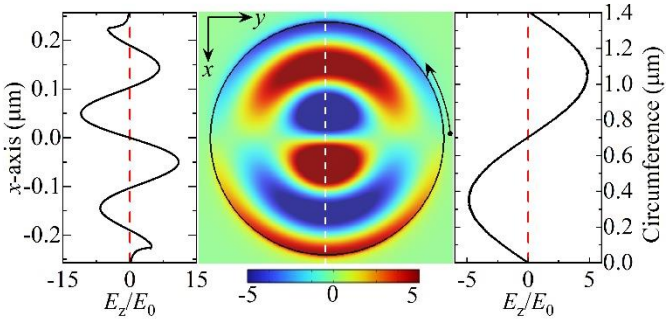

Fig. S3. Distributions of the normalized electric field E_z component along the (left) *x*-axis and (right) circumference for solid GSP resonator, adopted from the field distribution at the center. The diameter of the disk is 450 nm and the resonance wavelength is 735 nm.

IV. INFLUENCE OF THE NANOSPLIT ASYMMETRY

The influence of the nanosplit asymmetry on the optical response of the considered GSP resonator is summarized in Fig. S4. Two cases of the asymmetry are discussed. In the first case, the *x*-coordinate of the left side of the nanosplit is fixed at -15 nm, and its width is set to g = 40 nm. This corresponds to the nanosplit center being shifted by 5 nm from the disk center. Note that the coordinate system origin coincides with the disk center. The comparison of the scattering cross-section (black, left axis) and normalized spacer total electromagnetic energy spectra (red, right axis) of the symmetric (g = 30) and asymmetric (g = 40) cases is shown in Fig. S4(a). Dashed lines denote the symmetric configuration, and solid lines denote the asymmetric configuration. The inset shows the cross-section of the GSP configuration in the *xz*-plane, where the arrow indicates the fixed left side of the split. It is observed that both the scattering cross-section and spacer energy spectra of the symmetric and asymmetric geometries are quite similar, indicating that a 10-nm variation of the split size practically does not affect the normalized energy accumulated in the spacer. However, one can observe a barely distinguishable second resonance appearing for each WGM. For instance, for (1,1) mode the resonance in the symmetric structure is at 1740 nm, whereas in the asymmetric structure, along with the main resonance at ~1710 nm, another peak at ~1634 nm is seen in the energy spectrum [solid red line in Fig. S4(a)]. A similar tendency is also observed for (1,3) and (1,5) WGMs near 1025 nm and 800 nm, respectively. The chosen value of the asymmetry is linked to the conventional FIB milling accuracy[3]. Hence, similar values of the Purcell factor will be obtained as in the symmetric configuration.

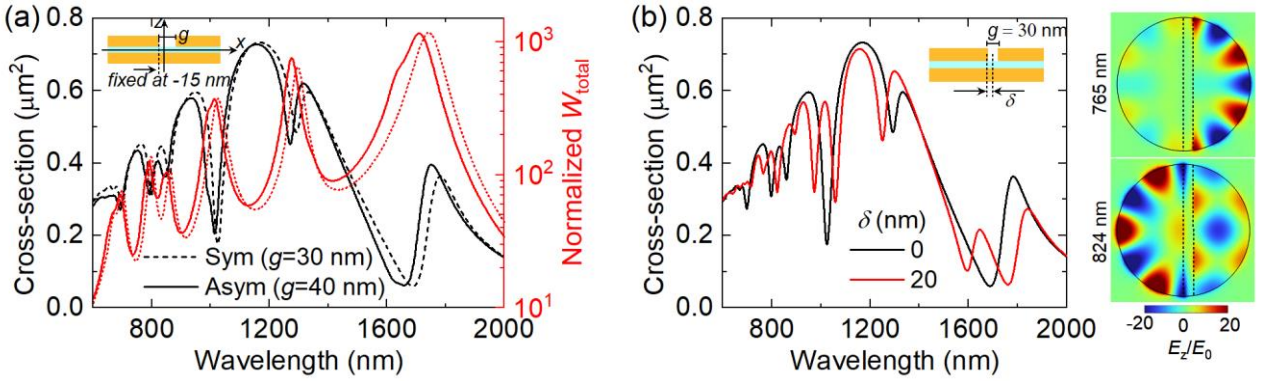

Fig. S4. (a) Scattering cross-section (left axis) and normalized total electromagnetic energy in the spacer (right axis) for symmetric (dashed lines) and asymmetric (solid lines) configurations, where the asymmetry is introduced by fixing the left side of the split and changing its width to g = 40 nm. The inset shows the xz cross-section of the configuration. (b) Comparison of the scattering cross-section spectra of symmetric and asymmetric configurations, where asymmetry is introduced by shifting the center of the 30-nm-wide split from the disk center by 20 nm. Right panel shows distributions of normalized amplitudes of the electric field E_z component of WGMs of the asymmetric configuration at 765 nm and 820 nm. This mode corresponds to (ℓ, m) = (1, 5) mode of the symmetric structure at 800 nm. In all cases the diameter of the disk is 450 nm and the spacer thickness is 10 nm.

In the next case, the nanosplit width is fixed at g = 30 nm, and the asymmetry is introduced by shifting its center by δ = 20 nm from the disk center along the separation (x) axis. The scattering cross-section spectrum of this configuration is compared with that of the symmetric one (the split and disk are concentric) in Fig. S4(b). Splitting of the resonance is now clearly observed for WGM-like modes, whereas other (hybrid) modes only experience some resonance shift. Right panel of Fig. S4 (b) illustrates distributions of normalized amplitudes of the electric field E_z component of WGMs of the asymmetric configuration at 765 nm and 820 nm. These modes correspond to (ℓ, m) = (1, 5) mode of the symmetric structure at 800 nm. The difference between the appearance of resonant splitting in two considered cases of asymmetry can be attributed to the size difference of two

hemicircular resonators, formed as a result of the shift between the split and disk centers. Particularly, in the first case, when the corner coordinate is fixed and the split width is set at 40 nm, the arc length of each part of the disk is 656.6 nm and 679.4 nm, whereas those in the second case are nearly 636.4 nm and 716.6 nm. Hence, the path difference of WGMs in each half of the disk is more pronounced in the second scenario (more than 3.5 times longer than that of the first scenario), resulting in clearly distinguishable resonances for each part of the disk.

The estimation for the *Q*-factor $m = 5$ mode shows that for the WGM at 765 nm, $Q \sim 45.5$, and for the WGM at 824 nm, $Q \sim 43.8$. These values are larger than that of the $m = 5$ WGM of the symmetric structure ($Q = 35.7$), which can be explained as follows: when WGMs are excited in the symmetric structure, charges with opposite polarity are induced along the nanosplit [see Fig. 4(e)]. The nanosplit itself acts as a Fabry-Perot resonator, supporting gap-plasmon modes with a dominant E_x component ($\lambda_{gsp}^{split} \sim 2/3D$, with D being the disk diameter), as also evidenced by the surface charge density distribution shown in Fig. 4(e). Importantly, the plasmonic WGMs of the spacer and the gap plasmons of the nanosplit are coupled, causing energy exchange and ultimately increasing the overall Ohmic losses in the system. However, when the asymmetric structure is considered, the WGMs are excited only in one half of the mode, and since there is no mode in the other half, the nanosplit mode is not excited.

V. ROLE OF THE SPACER DIELECTRIC

The confinement of the WGMs can be controlled by altering either the geometry or the spacer material of the split GSP resonator. The first mechanism involves manipulating the effective refractive index of modes by reducing the dielectric spacer thickness[4]. Alternatively, another material with a higher refractive index can be used as a spacer. To reveal the role of the high-index spacer on the optical response, we compared spectra of the scattering cross-section and total electromagnetic energy accumulated in the spacer of the split GSP resonators with SiO_2[5] and TiO_2[6] used as a dielectric. The results are shown in Fig. S5. A noticeable red shift of the optical response and an increase in the accumulated energy in the spacer are seen when TiO_2 is used as a spacer ($n \sim 2.3$ in the visible-NIR spectrum). Particularly, the resonance wavelength of the (5,1) mode is shifted from 800 nm (SiO_2) to 1080 nm (TiO_2). The normalised total electromagnetic energy accumulated in the spacer increases from 134 (SiO_2) to 315 (TiO_2).

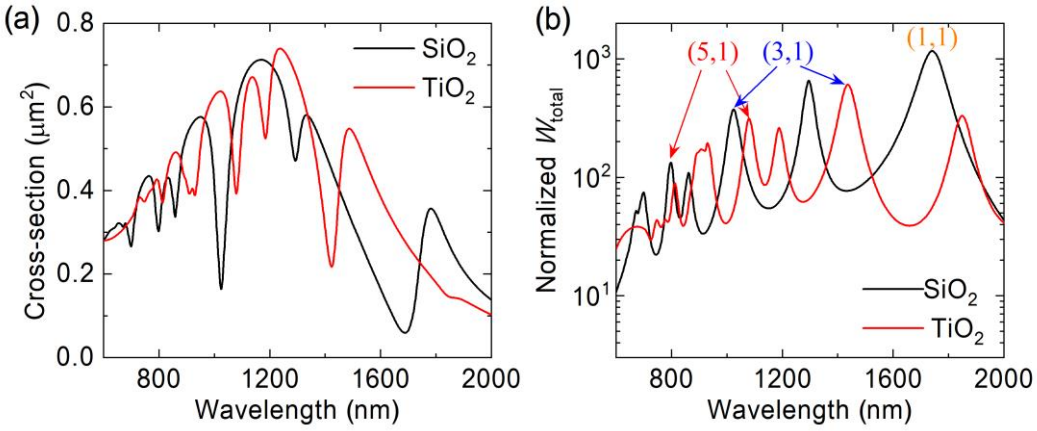

Fig. S5. (a) Scattering cross-section and (b) normalized total electromagnetic energy in the spacer for the split GSP resonator with SiO_2 (black) and TiO_2 (red) used as a spacer. The diameter of the disk is 450 nm and the spacer thickness is 10 nm.

References

1 R. Alaee, C. Rockstuhl and I. Fernandez-Corbaton, *Opt. Commun.*, 2018, **407**, 17–21.

2 T. Yezekyan, V. A. Zenin, J. Beermann and S. I. Bozhevolnyi, *Nano Lett.*, 2022, **22**, 6098–6104.

3 K. Höflich, G. Hobler, F. I. Allen, T. Wirtz, G. Rius, L. McElwee-White, A. V. Krasheninnikov, M. Schmidt, I. Utke, N. Klingner, M. Osenberg, R. Córdoba, F. Djurabekova, I. Manke, P. Moll, M. Manoccio, J. M. De Teresa, L. Bischoff, J. Michler, O. De Castro, A. Delobbe, P. Dunne, O. V. Dobrovolskiy, N. Frese, A. Gölzhäuser, P. Mazarov, D. Koelle, W. Möller, F. Pérez-Murano, P. Philipp, F. Vollnhals and G. Hlawacek, *Appl. Phys. Rev.*, , DOI:10.1063/5.0162597.

4 H. T. Miyazaki and Y. Kurokawa, *Phys. Rev. Lett.*, 2006, **96**, 097401.

5 L. Gao, F. Lemarchand and M. Lequime, *Opt. Express*, 2012, **20**, 15734.

6 T. Siefke, S. Kroker, K. Pfeiffer, O. Puffky, K. Dietrich, D. Franta, I. Ohlídal, A. Szeghalmi, E. Kley and A. Tünnermann, *Adv. Opt. Mater.*, 2016, **4**, 1780–1786.